Physics Letters B 684 (2010) 205–210

Contents lists available at ScienceDirect

Physics Letters B

www.elsevier.com/locate/physletb

Secondary scintillation yield in high-pressure xenon gas for neutrinoless double beta decay ($0\nu\beta\beta$) search

E.D.C. Freitas [a], C.M.B. Monteiro [a], M. Ball [b], J.J. Gómez-Cadenas [b], J.A.M. Lopes [a,c], T. Lux [d], F. Sánchez [d], J.M.F. dos Santos [a,*]

[a] GIAN-CI, Departamento de Física da Universidade de Coimbra, 3004-516 Coimbra, Portugal
[b] Instituto de Física Corpuscular (IFIC), CSIC – Universidad de Valencia, Valencia, Spain
[c] Instituto Superior de Engenharia de Coimbra, 3030-199 Coimbra, Portugal
[d] Institut de Fisica d'Altes Energies, Campus UAB, E-08193 Cerdanyola del Vallés, Barcelona, Spain

ARTICLE INFO

Article history:
Received 15 August 2009
Received in revised form 15 December 2009
Accepted 8 January 2010
Available online 16 January 2010
Editor: W. Haxton

Keywords:
Neutrino
Neutrinoless double-beta decay
Secondary scintillation
Xenon
High-pressure

ABSTRACT

The search for neutrinoless double beta decay ($0\nu\beta\beta$) is an important topic in contemporary physics with many active experiments. New projects are planning to use high-pressure xenon gas as both source and detection medium. The secondary scintillation processes available in noble gases permit large amplification with negligible statistical fluctuations, offering the prospect of energy resolution approaching the Fano factor limit. This Letter reports results for xenon secondary scintillation yield, at room temperature, as a function of electric field in the gas scintillation gap for pressures ranging from 2 to 10 bar. A Large Area Avalanche Photodiode (LAAPD) collected the VUV secondary scintillation produced in the gas. X-rays directly absorbed in the LAAPD are used as a reference for determining the number of charge carriers produced by the scintillation pulse and, hence, the number of photons impinging the LAAPD. The number of photons produced per drifting electron and per kilovolt, the so-called scintillation amplification parameter, displays a small increase with pressure, ranging from 141 ± 6 at 2 bar to 170 ± 10 at 8 bar. In our setup, this parameter does not increase above 8 bar due to non-negligible electron attachment. The results are in good agreement with those presented in the literature in the 1 to 3 bar range. The increase of the scintillation amplification parameter with pressure for high gas densities has been also observed in former work at cryogenic temperatures.

1. Introduction

Experiments searching for $\beta\beta$-decay have been ongoing for many decades. However, with the observation of the neutrino oscillations, one requirement for neutrino-less double beta decay has been met, a non-zero mass exists for at least one neutrino state. If the neutrino is a Majorana particle, meaning that neutrino and antineutrino are the same state, i.e. are not distinguishable by an extra quantum number then, and only then, it is possible for neutrinoless double-beta decay ($0\nu\beta\beta$) to occur. The unambiguous observation of this decay would demonstrate leptonic number violation and prove the Majorana nature of the neutrino. The detection of $0\nu\beta\beta$ would represent a breakthrough of new physics, beyond the Standard Model.

The search for $0\nu\beta\beta$ with various techniques is now increasingly intensive, and recent developments in detector technology make the observation of $0\nu\beta\beta$ feasible at the sensitivity scale required to address the question of normal or inverted hierarchy. A very recent detailed review of the $0\nu\beta\beta$, including active and planned experiments, is presented in [1].

The search for $0\nu\beta\beta$ processes is being carried out with different techniques. Germanium calorimeters were proposed for this purpose for the first time by [2] and used since then in experiments like Heidelberg-Moscow [3], IGEX [4], GEM [5], GENIUS [6] and GERDA [7]. Cryogenic TeO_2 bolometers are used in CUORE [8] and its smaller prototype, CUORICINO [9]. Others include tracking, such as the NEMO series [10], using a 3-D readout wire drift chamber.

A very interesting isotope for $0\nu\beta\beta$ experiments is ^{136}Xe [11], offering several advantages. As a noble gas, xenon can be used for tracking particles. It does not have long-lived radioactive isotopes other than ^{136}Xe, which decays by $\beta\beta$. The ^{136}Xe fraction can be easily enriched to high concentrations by centrifugation methods. The Q-value of the $^{136}\text{Xe} \rightarrow {}^{136}\text{Ba}$ transition is 2457 keV, among the higher values of potential $0\nu\beta\beta$ candidates. The $2\nu\beta\beta$ may be as long as 10^{22}–10^{23} years [12], while the $0\nu\beta\beta$ is predicted to be equivalent to the one of ^{76}Ge. Furthermore, xenon can be used as source and detector material. The EXO Collaboration has cho-

* Corresponding author.
E-mail address: jmf@gian.fis.uc.pt (J.M.F. dos Santos).

0370-2693/$ – see front matter
doi:10.1016/j.physletb.2010.01.013

sen a Liquid Xenon (LXe) TPC as their detector [13]. Liquid xenon, dissolved in scintillator is also being proposed by the KAMLAND Collaboration [14]. A LXe detector, such as EXO, has the advantages of being compact and self-shielding.

However, there are some detector features that are essential for a $0\nu\beta\beta$ experiment to succeed. The impact of background in a $0\nu\beta\beta$ experiment depends strongly on the energy resolution, which is essential not only to reduce the tail of the $2\nu\beta\beta$ spectrum from overlapping the region of interest of the $0\nu\beta\beta$ spectrum, but also to prevent the contamination of the region of Interest (ROI) by the more dangerous background from the 2.6 MeV gamma emanating from ^{206}Tl and 2.4 MeV gamma from ^{214}Bi. Furthermore, external backgrounds should also be reduced using topological properties of the $0\nu\beta\beta$ events. The two-electron signature of the $\beta\beta$ decay can suppress any background from the Tl and Bi gammas contaminating the ROI.

The NEXT Collaboration [15] considers that High Pressure Gaseous Xenon (HPXe) may be a better solution than LXe for these two reasons, energy resolution and event topology. Energy resolution in LXe is mediocre, of the order of 4–5% FWHM at $Q_{\beta\beta}$ [13,16,17], while measurements in HPXe indicate an intrinsic resolution of 0.4% at $Q_{\beta\beta}$ from charge alone. In addition, HPXe will be sensitive to the topological signature of the two electrons, as demonstrated by the Gottard TPC [12] and discussed at length in the NEXT proposal [15]. In LXe, both the Compton tail from the 2.6 MeV ^{206}Tl gamma and the photoelectric peak from the 2.4 MeV ^{214}Bi gamma contaminate the large ROI (due to mediocre energy resolution). Those gammas are, in general, not resolved from the two-electron signature arising from $\beta\beta$ processes due to the high density of liquid xenon, causing signal and background to be observed as single blobs. Instead, in HPXe, the number of these gammas contaminating the ROI is reasonably expected to be much smaller and is further suppressed due to the observation of a single-electron signature, distinctly different from the two-electron signature [15].

For half a century [18,19] it has been known that secondary scintillation, also called electroluminescence, provides signals with much larger amplitudes, minimal fluctuations in gain and negligible electronic noise, being the optimum amplification technique for this kind of experiments [20]. Therefore, especially in experiments with very low event rates and/or high background levels, as are the $0\nu\beta\beta$ experiments, it is of great importance to use the secondary scintillation signal rather than the signal from either unamplified primary ionization or secondary ionization [20]. This is the technique to be used in NEXT, with a nominal xenon pressure of 10 bar [15]. A similar project has been submitted to SNO Lab by the EXO Collaboration [21].

Recently, we measured absolute electroluminescence yields of xenon [22,23] and argon [24], around atmospheric pressure, with a simple method that makes use of just one experimental setup, without the need for calibration/comparison procedures that are sometimes difficult to carry out and often a source of additional errors. This method has been extensively used to measure the primary scintillation yield in inorganic crystals [25] and we have already used it as well for the determination of the secondary scintillation yield in xenon [22]. The results we obtained were in very good agreement, both with experimental results from other groups as well as with Monte Carlo simulation studies and Boltzmann calculations ([22] and references therein), which brings out the reliability of the method. A VUV-sensitive Large Area Avalanche Photodiode (LAAPD) is used to detect, simultaneously, the secondary scintillation of a gas proportional scintillation counter (GPSC) and incident X-rays. The X-rays are used as a reference for determining the absolute number of VUV-photons impinging the LAAPD [25].

As the electroluminescence yield is defined as the number of photons produced in the scintillation gap per electron crossing the scintillation gap and per unit of path, we used X-rays to create a known number of primary electrons in xenon. The interaction of the X-rays in xenon has been extensively studied and the number of electrons resulting from the X-ray interaction is well known. In addition, X-rays have been used extensively as a reference to calibrate the number of charge carriers produced in avalanche photodiodes.

For high pressures there are no studies reported in the literature. Favata et al. [26], concluded that the reduced electroluminescence yield is pressure-independent, in the region of 1 to 2 bar. Fonseca et al. [27], have shown that the scintillation yield increases only slightly for gas temperature in the range from 20 down to −88 °C and 2 bar pressure (corresponding to 3.2 bar PTN) but, on the other hand, for −90 °C and 2 bar, near the xenon saturation point, the scintillation amplification factor varies significantly.

This gave us the motivation to investigate the behaviour of the xenon electroluminescence yield at high-pressures. In this work, the xenon electroluminescence yield is studied as a function of electric field in the scintillation region, for xenon pressures from 2 to 10 bar, using the same method applied in [22–24].

2. Experimental setup

Fig. 1 depicts the schematic of the GPSC used in this work, which is the same system used in [28]. The detector body has a cylindrical shape with 9 cm in diameter and 3.5 cm in height. Mesh G1 holder is a stainless steel cylinder of 4 cm diameter, and has multiple perforations on its side surface to increase gas circulation in the drift/absorption region.

The radiation window is kept at negative high-voltage −HV0, while mesh G1 and its holder are kept at −HV1; mesh G2 and detector body are grounded. Electrical insulation of the radiation window and the G1 holder is achieved using a machineable glass-ceramic, Macor®, glued to the detector body and to the window with a low vapour pressure epoxy. The voltage difference between the detector window and G1 defines the reduced electric field in the absorption/drift region, which is kept below the xenon scintillation threshold, $\sim 0.8\ \mathrm{kV\,cm^{-1}\,bar^{-1}}$, throughout the work. The scintillation region is delimited by G1 and G2. The electric field in this region is defined by −HV1. In this GPSC prototype, the absorption/drift region and the scintillation region were designed to be shallow (1-cm deep and 1.5-mm deep, respectively), to keep high reduced electric fields (electric field intensity divided by the gas pressure, E/p) with relatively low biasing-voltages.

Maximum HV0 and HV1 values vary from 3.3 and 1.9 kV to 11.0 and 3.4 kV, as the pressure rises from 2 to 10 bar, respectively. For each pressure, the maximum achieved E/p was limited by electrical insulation and maintained below the onset of electric breakdown, i.e. the appearance of microdischarges, noticeable in the oscilloscope and in the MCA during the pulse-height distribution acquisition.

The LAAPD is a custom made API Deep-UV model with a 16-mm diameter active area [29]. In order to have equal pressure on both sides of the silicon wafer, the LAAPD has several holes 3-mm in diameter throughout its body, connecting the outer surface to the inner chamber, which encloses the electrical contacts with the SHV socket. Throughout this work, the LAAPD biasing was set to a safe value of 1650 V, corresponding to a photosensor gain of 25 [29]. Although this gain is low, high performance is already reached as a result of both high scintillation amplification in the GPSC and high conversion-efficiency of xenon scintillation into charge in the LAAPD [30].

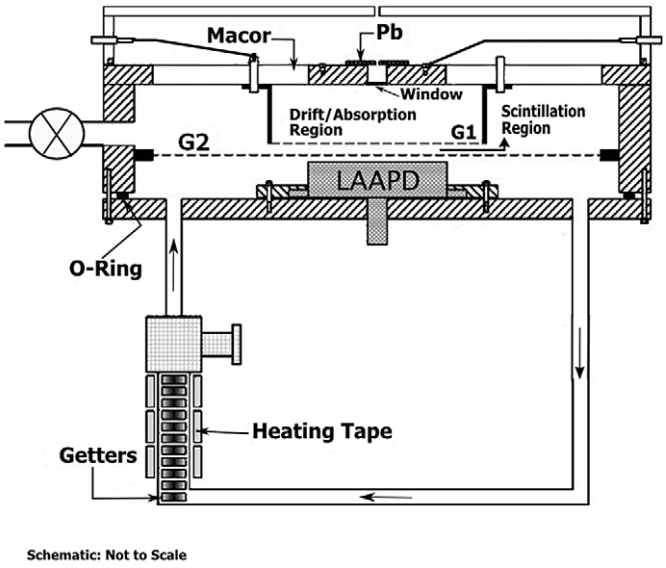

Fig. 1. Schematic of the GPSC instrumented with a LAAPD substituting for the PMT.

The detector was filled with xenon at pressures up to 10 bar and the pressure was kept constant during each set of measurements. Xenon circulates through convection, while continuously purified, by non-evaporable getters (SAES Getters, St 707/washer/833) that are kept at a stable temperature in the range 100–250 °C.

The charge signals of the LAAPD were fed through a CANBERRA 2006 charge-to-voltage preamplifier (sensitivity of 235 mV/10^6 ion pairs) and a TENNELEC TC243 linear amplifier (1-μs peaking time constant) to a 1024-multichannel analyser. For peak amplitude and energy-resolution measurements, pulse-height distributions were fitted to a Gaussian function superimposed on a linear background, from which the centroid and the FWHM were determined.

3. Method

Upon crossing the scintillation region, the primary electrons gain from the electric field enough energy to excite but not ionise the xenon atoms. As a result of subsequent excimer formation and de-excitation processes, a strong scintillation pulse is generated. The processes leading to emission in the second continuum occur through three-body collisions and can be schematized by

$$\mathrm{Xe}^* + 2\mathrm{Xe} \rightarrow \mathrm{Xe}_2^* + \mathrm{Xe},$$

$$\mathrm{Xe}_2^* \rightarrow 2\mathrm{Xe} + h\upsilon.$$

One excited atom creates an excited excimer, Xe_2^*, which decays emitting one VUV photon, $h\upsilon$. For pressures above a few tenths of bar the electroluminescence spectrum of xenon consists of a narrow line peaking at 172 nm, with 5 nm FWHM [31], the second continuum. The spectrum corresponds to transitions of the singlet and triplet bound molecular states, from vibrationally relaxed levels, to the repulsive ground state.

The electroluminescence yield, Y, is defined as the number of secondary scintillation photons produced per drifting primary electron per unit path length, d

$$Y = \frac{N_{UV}}{d \times T} \times \frac{4\pi}{\Omega_{Sc}} \times \left(\frac{E_X}{w_{E_X}}\right)^{-1}, \tag{1}$$

where N_{UV} is the number of VUV-photons impinging the LAAPD per X-ray absorbed in the xenon drift gap, T is the transmission of the grid (84%), Ω_{Sc} is the average solid angle subtended by the LAAPD, E_X is the energy of the incident X-ray and w_{E_X} the respective w-value for xenon. For our LAAPDs, the manufacturer provided a $QE \sim 1.1$ for the number of charge carriers produced in the LAAPD per incident 172-nm VUV photons [30,32]. According to the manufacturer, the LAAPD fabrication technology is well established, and quite good reproducibility is obtained. Therefore, the behaviour observed for individual LAAPDs is expected to be representative for any of these devices, with an uncertainty in QE of about ±10% [33]. The average solid angle, Ω_{Sc}, subtended by the active area of the LAAPD for the primary electron path has been computed by Monte Carlo simulation [34]. A value of 4.3 ± 1 sterad was obtained. The w-value for xenon, 21.7 eV for 22.1 and 59.6 keV X-rays, was obtained from [35]. Beside the uncertainty in QE, another dominating source of uncertainty in the calculated yield is the scintillation gap thickness, d, which is limited by the mechanical precision, estimated in, at most, 150 μm, i.e. ±10% relative error for the scintillation gap thickness. A direct comparison between the amplitudes of the electroluminescence, A_{Sc}, and the X-rays directly absorbed in the LAAPD, A_X, provides a quantification for N_{UV},

$$N_{UV} = \frac{A_{Sc}}{A_X} \times \frac{N_{e,XR}}{QE} \text{ photons}, \tag{2}$$

being $N_{e,XR}$ the number of charge carriers produced in the LAAPD by the direct X-ray interaction. A_{Sc} and A_X are obtained from the pulse height distributions biasing the whole GPSC or only the LAAPD, respectively. $N_{e,XR}$ is calculated from

$$N_{e,XR} = \frac{E_x}{w_{Si}} \text{ electrons}, \tag{3}$$

where E_x is the energy of the incident X-ray and w_{Si} the respective w-value for silicon. A_{Sc} and A_X are obtained with a precision better than ±1% and ±2%, respectively. Therefore, the uncertainty obtained for the yield is within ±15%.

4. Results and discussion

Fig. 2 depicts pulse-height distributions obtained with LAAPD readout for the electroluminescence pulses resulting from ^{109}Cd X-rays interacting in xenon and for the X-rays directly interacting in the LAAPD. Fig. 2(b) depicts the pulse-height distributions resulting from X-rays directly interacting in the LAAPD. As shown, pulse-amplitudes resulting from electroluminescence depend on the electric field applied to the scintillation region, while pulse-amplitudes resulting from X-rays directly interacting in the LAAPD are independent from drift and scintillation region biasing, depending only on the LAAPD biasing.

In Fig. 3 we depict the reduced electroluminescence yield, Y/p, i.e. the electroluminescence yield divided by the gas pressure as a function of reduced electric field, E/p, in the scintillation region, for pressures up to 10 bar, using 22.1 (Fig. 3(a)) and 59.6 keV (Fig. 3(b)) photons. The data illustrate the characteristic approximately linear trend of electroluminescence dependence on the reduced electric field, having a scintillation threshold around 0.8 kV cm^{-1} bar^{-1}. As an example, for the 2 bar curve in Fig. 3(a),

$$Y/p\ \left(\text{photons electron}^{-1}\,\text{cm}^{-1}\,\text{bar}^{-1}\right) = 151E/p - 131, \tag{4}$$

where E/p is given in kV cm^{-1} bar^{-1}, or

$$Y/N\ \left(10^{-17}\ \text{photons electron}^{-1}\,\text{cm}^2\,\text{atom}^{-1}\right) = 0.151 \times E/N - 0.530, \tag{5}$$

where E/N is given in Td (10^{-17} V cm^2 atom^{-1}), in density units.

In Table 1 we list the scintillation amplification parameter, i.e. the number of photons produced per drifting electron and per kilovolt, the slope of the linear trend, obtained for the different xenon

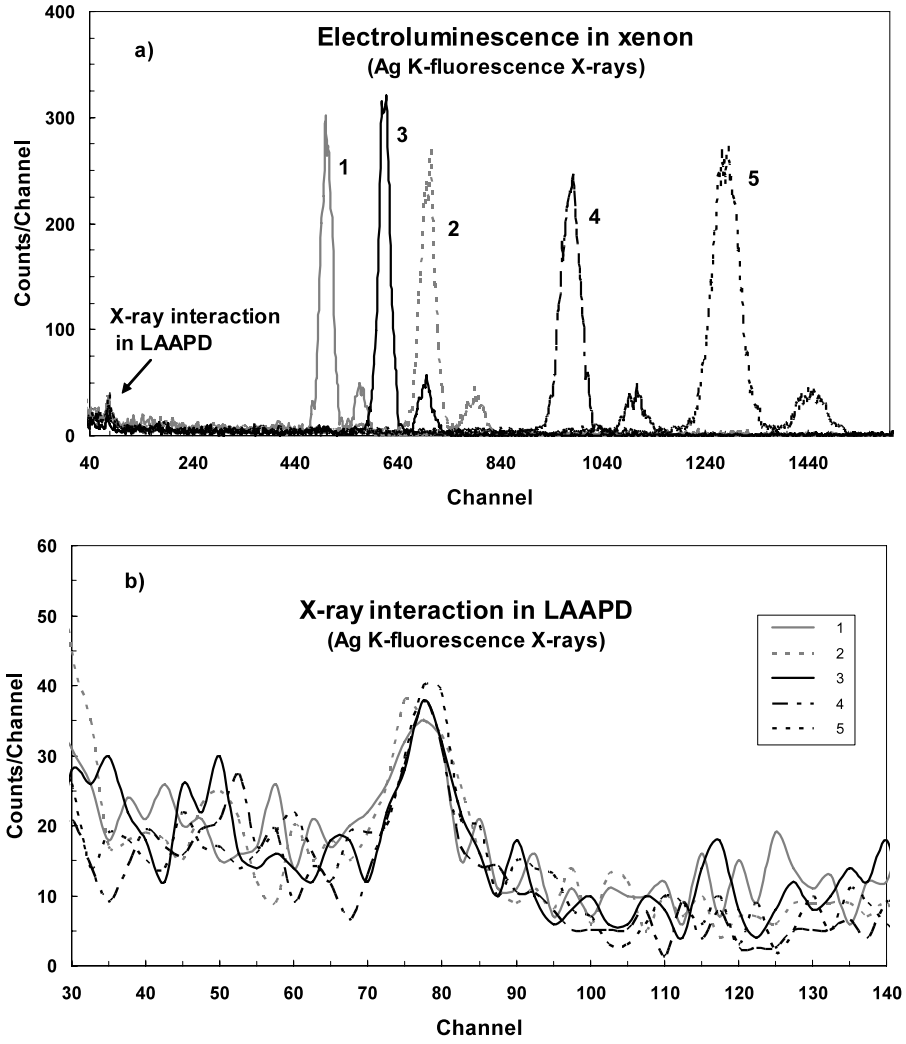

Fig. 2. (a) Pulse-height distributions from LAAPD readout for electroluminescence resulting from ^{109}Cd X-rays interacting in xenon and for X-rays directly interacting in the LAAPD. (b) details the pulse-height distributions from X-rays directly interacting in the LAAPD. Legend: 1: 2 bar, $E/p = 4.8$ kV cm^{-1} bar^{-1}; 2: 2 bar, $E/p = 6.2$ kV cm^{-1} bar^{-1}; 3: 4 bar, $E/p = 3.0$ kV cm^{-1} bar^{-1}; 4: 4 bar, $E/p = 4.4$ kV cm^{-1} bar^{-1}; 5: 4 bar, $E/p = 5.3$ kV cm^{-1} bar^{-1}.

pressures. The results agree with those obtained in [22] at 1 bar. The scintillation amplification parameter shows a small increase with pressure, of about 20%. This trend has been observed at cryogenic temperatures for high gas densities [27]. For pressures above 8 bar the increase is marginal; we attribute this effect to non-negligible electron attachment that may occur at higher densities [36]. This effect also explains the degradation in the energy resolution of our detector for higher pressures [28]. The results obtained with the setup of [37], in the range of 2–5 bar and using 5.9-, 22.1- and 59.5-keV X-rays, have been analyzed using the above described method, rendering values that agree, within errors, with those obtained with the present setup. The former have also been used for the calculation of the average amplification parameters and respective errors, presented in Table 1. For each run, e.g. the results presented for 2 bar in Fig. 3(a), a value for the amplification parameter and respective error is obtained from a linear fit to the data points. The final amplification parameter and error, presented in Table 1, are determined by weighing averages and respective errors of the different runs performed for each pressure. The differences in errors for the different pressures are mainly due to the number of runs performed for each pressure, e.g. only 2 runs for 6, 8 and 10 bar, while for 2, 4 and 5 bar, 5 runs were performed. We have fit the amplification parameter limiting the range of the reduced electric field in the scintillation region to 3 kV cm^{-1} bar^{-1} for all pressures, with similar results.

The primary scintillation is separated in time from the secondary scintillation by less than one microsecond, the electron drift time while crossing the drift region. Nevertheless, the number of primary scintillation photons is more than three orders of magnitude lower than that of the secondary scintillation and, therefore, quite negligible.

5. Conclusions

We have measured the xenon reduced electroluminescence yield, i.e. the number of secondary scintillation photons produced per drifting primary electron per unit path length, as a function of the reduced electric field, for different pressures between 2 and 10 bar. The measurements were performed using a gas proportional scintillation counter (GPSC) instrumented with a large area avalanche photodiode for the electroluminescence readout. Direct interactions of 22.1 keV X-rays in the LAAPD were used as a reference for the determination of the number of charge carriers produced by the scintillation pulse and, thus, the number of VUV photons impinging the photodiode, given its quantum efficiency.

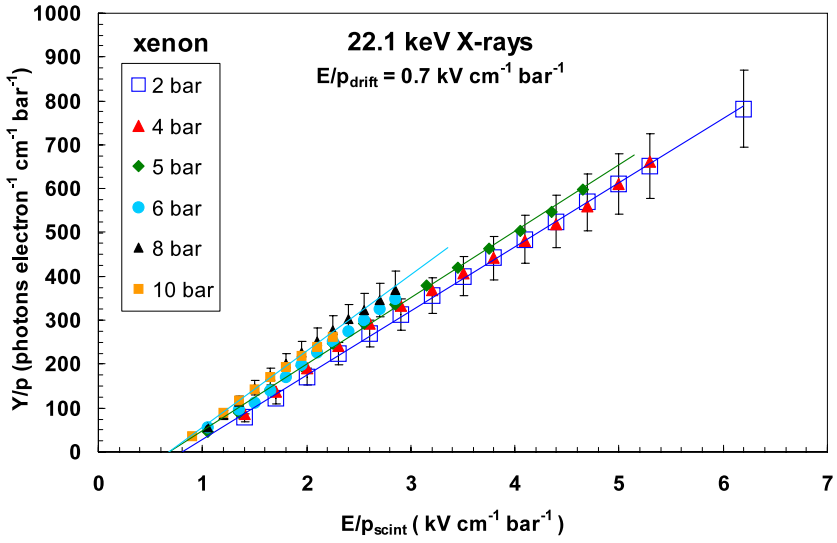

(a)

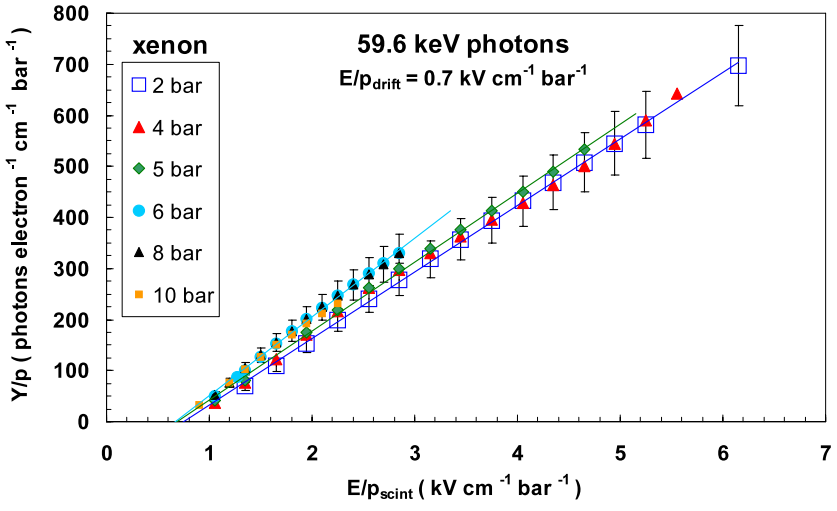

(b)

Fig. 3. Xenon reduced electroluminescence yield as a function of reduced electric field, for different pressures, as measured using 22.1 and 59.6 keV photons. Trend lines are included only to guide the eye.

Table 1
Xenon scintillation amplification parameter for pressures ranging from 2 to 10 bar.

Pressure (bar)	2	3	4	5	6	8	10
Scintillation Amplification Parameter (photons e^{-1} kV^{-1})	141 ± 6	141 ± 7	142 ± 5	151 ± 5	161 ± 9	170 ± 10	162 ± 10

The measurements have shown that the number of photons produced per drifting electron and per kilovolt, the so-called scintillation amplification parameter, presents a small increase with pressure, increasing from 141 ± 6 at 2 bar to 170 ± 10 at 8 bar. The increase with pressure is significant since most of the systematic errors are common to both points. Above 8 bar it does not increase; we attribute this effect to non-negligible electron attachment that occurs at higher densities. The results are in good agreement with former results presented in the literature in the 1 to 3 bar range. The increase of the scintillation amplification parameter with pressure for high gas densities was also observed in former work at cryogenic temperatures.

Acknowledgements

This work was supported by Project PTDC/FIS/103860/2008 through FCT and FEDER programs. The spanish authors acknowledge the support of the CONSOLIDER-INGENO 2010 project CUP (CSD2008-00037). E.D.C. Freitas acknowledges grant SFRH/BD/46711/2008. C.M.B. Monteiro acknowledges grant SFRH/BD/25569/2005. This work is supported by Spanish Ministerio de Educación y Ciencias under grants FPA2006-12120-C03-01 and FPA2006-12120-C03-03 with partial support from FEDER program. Thanks are due to Sonja A. Orrigo (CI – University of Coimbra) for her help with

the linear fit analysis using PAW and to D. Nygren (LBNL, USA) for style revision.

References

[1] F.T. Avignone, et al., Rev. Mod. Phys. 80 (2008) 481.
[2] E. Fiorini, et al., Phys. Lett. B 25 (1967) 602.
[3] H.V. Klapdor-Kleingrothaus, et al., Eur. Phys. J. A 12 (2001) 147.
[4] C.E. Aalseth, et al., Phys. Rev. D 70 (2004) 078302, http://arxiv.org/abs/nucl-ex/0404036v2.
[5] Yu.G. Zdesenko, et al., J. Phys. G 27 (2001) 2129.
[6] H.V. Klapdor-Kleingrothaus, Nucl. Phys. B (Proc. Suppl.) 110 (2002) 364.
[7] S. Schönert, et al., Phys. At. Nucl. 69 (2006) 2101.
[8] M. Pedretti, et al., Int. J. Mod. Phys. A 23 (2008) 3395.
[9] C. Arnaboldi, et al., Phys. Rev. C 78 (2008) 035502.
[10] R. Arnold, et al., Nucl. Phys. A 781 (2007) 209.
[11] M.K. Moe, Phys. Rev. C 44 (1991) R931.
[12] R. Luescher, et al., Phys. Lett. B 434 (1998) 407.
[13] D.S. Leonard, et al., Nucl. Instrum. Methods A 591 (2008) 490.
[14] M. Koga, The future project of KamLAND (Neutrino-less double beta decay experiment on KamLAND), Workshop on Xenon-Based Detectors, Berkeley, USA, 16–18 November 2009; http://indico.cern.ch/conferenceOtherViews.py?view=standard&confId=66513.
[15] F. Grañena, et al., NEXT Collaboration, NEXT Letter of Intent, Laboratorio Subterráneo de Canfranc EXP-05.
[16] A. Bolotnikov, B. Ramsey, Nucl. Instrum. Methods A 396 (1997) 360.
[17] E. Conti, et al., Phys. Rev. B 68 (2003) 054201.
[18] C.A.N. Conde, A.J.P.L. Policarpo, Nucl. Instrum. Methods 53 (1967) 7.
[19] A.S. Conceição, et al., JINST 2 (2007) P09010.
[20] D. Nygren, Nucl. Instrum. Methods A 581 (2007) 632.
[21] D. Sinclair, Progress on a Gaseous Xe detector for Double Beta Decay (EXO), Workshop on Xenon-Based Detectors, Berkeley, USA, 16–18 November 2009; http://indico.cern.ch/conferenceOtherViews.py?view=standard&confId=66513.
[22] C.M.B. Monteiro, et al., J. Inst. 2 (2007) P05001.
[23] C.M.B. Monteiro, et al., Phys. Lett. B 677 (2009) 133.
[24] C.M.B. Monteiro, et al., Phys. Lett. B 668 (2008) 167.
[25] M. Moszynski, et al., Nucl. Instrum. Methods A 485 (2002) 504.
[26] F. Favata, et al., Nucl. Instrum. Methods A 294 (1990) 595.
[27] A.C. Fonseca, et al., 2004 IEEE Nucl. Sci. Symp. Conference Record (2005).
[28] L.C.C. Coelho, et al., Nucl. Instrum. Methods A 575 (2007) 444.
[29] U.V. Deep, 500 Windowless Series LAAPD, Advanced Photonics Inc., Camarillo, CA.
[30] J.A.M. Lopes, et al., IEEE Trans. Nucl. Sci. 48 (2001) 312.
[31] T. Takahashi, et al., Nucl. Instrum. Methods 205 (1983) 591.
[32] B. Zhou, M. Szawlowski, An explanation on the APD spectral quantum efficiency in the deep UV range, Interoffice Memo, Advanced Photonix Inc., 1240 Avenida Acaso, Camarillo, CA 93012, EUA, 1999.
[33] M. Szawlowski, Advanced Photonix Inc., private communication (2002).
[34] J.M.F. dos Santos, et al., IEEE Trans. Nucl. Sci. 39 (1992) 541.
[35] T.H.V.T. Dias, et al., J. Appl. Phys. 82 (1997) 2742.
[36] A. Bolozdynya, et al., Nucl. Instrum. Methods A 385 (1997) 225.
[37] D.S. Covita, et al., IEEE Trans. Nucl. Sci. 51 (2004) 1492.